Hindawi
Advances in Mathematical Physics
Volume 2019, Article ID 6865730, 12 pages
https://doi.org/10.1155/2019/6865730

Research Article

A Continuum Approach to the Nonlinear In-Plane Galloping of Shallow Flexible Cables

M. Ferretti,[1,2] **D. Zulli**,[1,2] **and A. Luongo**[1,2]

[1]*International Research Center on Mathematics and Mechanics of Complex Systems, University of L' Aquila, 67100 L' Aquila, Italy*
[2]*Department of Civil, Construction-Architectural and Environmental Engineering, University of L' Aquila, 67100 L' Aquila, Italy*

Correspondence should be addressed to A. Luongo; angelo.luongo@univaq.it

Received 31 October 2018; Accepted 13 January 2019; Published 14 March 2019

Academic Editor: Zine El Abiddine Fellah

The aeroelastic stability of horizontal, suspended, shallow, iced cables is studied via a continuum model. Both external and internal damping, consistent with the Rayleigh model, are taken into account. The quasi-static theory of the aerodynamic forces is applied. An in-plane nonlinear model of galloping is formulated, displaying the importance of internal damping, both on the critical velocity and on the limit-cycle amplitude. A perturbation procedure is developed for nonlinear analysis in nonresonant conditions (monomodal galloping). The modification of the galloping mode due to quadratic nonlinearities is studied, and its real or complex character is discussed.

1. Introduction

Cables are slender structures that can significantly suffer wind effects. For instance, in cold regions, those structures might undergo galloping, resulting in large vibrations at low frequencies. The phenomenon is indeed associated with the wind interacting with noncircular cable cross-sections, as molded by ice or sleet accretions. In [1], the triggering of galloping is addressed with reference to a reduced mechanical model of cable, in response to vanishing of the total damping of the structure, which is the sum of both mechanical and aerodynamic contributions. Recently, richer models have been developed, e.g., taking into account coupled in-plane and out-of-plane motions to analyze the incipient instability [2] or considering nonlinear effects to address the postcritical behavior [3]. In some cases, the contribution of the twist and bending of the cable is taken into account, in order to consider the complete stiffness amount furnished by the structure [4]; there, continuum models of cables are used and then reduced via Galerkin projections to few degrees of freedom (d.o.f.) systems. In [5], a direct approach to the nonlinear problem, based on a continuum model of cable, is proposed; there, referring to classical flexible models [6–8], the mechanical damping of the cable is considered as an external contribution, i.e., proportional to the cable velocity and related to the energy dissipation due to the interaction of the structure with the surrounding fluid. However, richer models of mechanical damping might be possibly proposed, where viscoelasticity of the structure material is taken into account, even in the linear field. For instance, this is easily done in case of beams [9, 10], where the Kelvin-Voigt rheological model is adopted and a strain-rate dependent term, proportional to the elastic stiffness and associated with internal energy dissipation, is introduced. Nevertheless, in case of cables, the problem is much more complicated, with the stiffness being of mixed type, i.e., of both elastic and geometrical kind. In particular, the elastic stiffness could still resort to the Kelvin-Voigt model. However, for the geometric stiffness, a more sophisticated micromechanical model should be developed, referring to the real geometry of the rope and accounting for the friction interactions which occur among the strands that constitute the cable. Such a model, unfortunately, is far from being developed in literature, even if a promising mechanical model for hysteretic damping on ropes was recently proposed [11].

In this paper, a continuum mechanical model of cable is considered where, besides the classical external damping, an internal damping contribution related to viscous effects is introduced. In the spirit of Rayleigh damping model, it is taken as proportional to the linear stiffness operator.

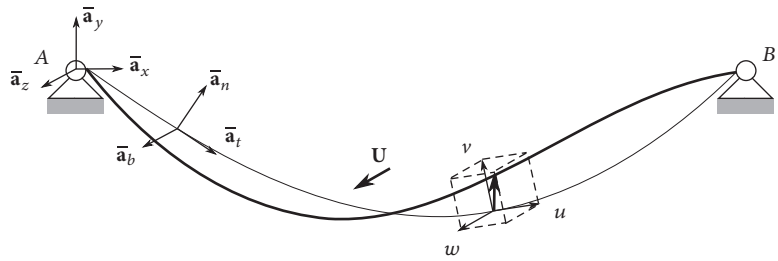

Figure 1: Shallow horizontal cable under normal wind flow. Thin line: in-plane equilibrium position under self-weight; thick line: current configuration under the action of both self-weight and wind.

Combined with the aerodynamic forces, formulated in the framework of the quasi-steady theory, the effect of both the damping contributions is addressed with reference to the galloping phenomenon. Dealing with cables far from the cross-over point [6], the critical conditions of monomodal galloping are evaluated from the linear problem. Then, the nonlinear problem is addressed via a perturbation method, namely, the multiple scale method (MSM) [12–14], in order to evaluate the postcritical behavior and the amplitude and shape of limit-cycle. Comparison is carried out via numerical integration of the equations relevant to two companion finite-dimensional models, one formulated with a multimode Galerkin projection, and the other with the finite difference method.

The paper is organized as follows: in Section 2 the mechanical and aerodynamic model of the cable is formulated; in Section 3 the linear problem is addressed and the critical conditions are evaluated; in Section 4 the nonlinear problem is dealt with; in Section 5 the finite-dimensional models are formulated; in Section 6 numerical outcomes are presented; and finally in Section 7 some conclusions are drawn.

2. Continuum Model

2.1. Formulation. We analyze galloping of iced, small-sag, horizontal cables. Under self-weight, the cable hangs on points A and B in the vertical plane, spanned by the unit vectors $(\bar{\mathbf{a}}_x, \bar{\mathbf{a}}_y)$, and occupies the equilibrium configuration shown in thin line in Figure 1. Possible evaluation of the equilibrium configuration via perturbation methods is discussed in [15, 16]. An orthogonal uniform wind $\mathbf{U} = U\bar{\mathbf{a}}_z$ is assumed to flow, which causes the cable to reach an unknown current configuration, shown in thick line in Figure 1. At the abscissa s and time t, the dynamic displacement due to the wind is described in the intrinsic basis $(\bar{\mathbf{a}}_t, \bar{\mathbf{a}}_n, \bar{\mathbf{a}}_b)$ by the tangential, normal (in-plane), and binormal (out-of-plane) components, referred to as $u(s,t), v(s,t), w(s,t)$, respectively.

The equations of motion of the cable, with the tangent displacement $u(s,t)$ condensed and flexural and torsional stiffness ignored, were derived, e.g., in [4] for the transverse motion $v(s,t), w(s,t)$. In particular, the static condensation of $u(s,t)$ is carried out under the reliable hypothesis of much larger celerity of the longitudinal waves with respect to the transverse ones [3, 6, 7, 17–19]. Here, however, we ignore the out-of-plane displacement $w(s,t)$, which was shown in the literature to weakly affect the galloping phenomenon (except in resonant cases, here excluded, [2]). Therefore, the equations ruling the in-plane motion read as follows.

$$\begin{aligned} &\left(T_0 + EAe\right) v'' + EA\bar{k}e - m\ddot{v} + f_n^d + f_n^a = 0 \\ &e = -\frac{\bar{k}}{l}\int_0^l v\,ds + \frac{1}{2l}\int_0^l v'^2 ds \\ &v_A = 0, \\ &v_B = 0 \end{aligned} \tag{1}$$

Here T_0 is the prestress, assumed constant on s; EA is the axial stiffness; m is the mass per unit length, possibly including the ice accretion; l is the length of the cable, taken nearly equal to the chord; $\bar{k} := mg/T_0$ is the prestress curvature, also assumed to be constant; $e(t)$ is the dynamic unit extension, constant on s, from which the dynamic tension is evaluated as $\widetilde{T} = EAe$; and f_n^d are damping forces and f_n^a aerodynamic forces, all per unit length, acting in the normal direction, respectively. Subscripts A and B indicate evaluation of the variable at the points A and B, namely, at $s = 0$ and $s = l$, respectively; finally, the dot stands for time-differentiation and the prime for s-differentiation.

2.2. Damping Model. In a galloping problem, it is mandatory accounting for damping. As is well known [20–22], there exist two forms of damping: an external damping, accounting for the medium resistance, and an internal damping, which describes various dissipation sources in the body via an 'equivalent' viscous mechanism. However, while it is easy to model linear external damping forces as proportional to velocities, i.e., $-c_e\dot{v}$, with $c_e > 0$ a damping coefficient, the same does not happen for internal damping. Indeed, differently from what happens in beams, in which the rheological Kelvin-Voigt model naturally leads to viscous operators proportional to the elastic stiffness operators [9], in cables such a similarity does not hold, since the relevant stiffness is of mixed nature, elastic and geometric. Concerning the elastic stiffness, by still resorting to Kelvin-Voigt model, a local force as $\eta A\bar{k}\dot{e}$ should be considered, with η a viscosity coefficient; concerning the geometric stiffness, a more sophisticated micromechanical model should be developed, referring to the real geometry of the rope and accounting for the friction interactions which occur among the strands that constitute

the cable. Such a model, unfortunately, is far from being developed in literature. By attributing the energy loss to an equivalent viscous mechanism, we could heuristically assume that internal damping actions are proportional to the rate of curvature of the cable, which is responsible for relative velocities among the strands, namely, $\zeta \dot{v}''$ with $\zeta > 0$ a second viscosity coefficient, independent of η, related to a different dissipation mechanism. Such a model, however, would lead to a nonproportional damping, with the occurrence of complex modes. As a first, rough approach to the problem, the Rayleigh model of damping [23] is adopted here, by assuming that η and ζ are related to each other, namely, $\eta/E = \zeta/T_0$. Accordingly, the internal damping operator is taken proportional to the linear stiffness operator (the external damping being proportional to the mass), namely,

$$f_n^d = -c_e \dot{v} + \zeta \left(\frac{EA}{T_0} \overline{k} \dot{e} + \dot{v}'' \right). \tag{2}$$

The equations of motion therefore read as follows.

$$\begin{aligned} & T_0 \left(1 + \frac{\zeta}{T_0} \partial_t \right) v'' + EA\overline{k} \left(1 + \frac{\zeta}{T_0} \partial_t \right) e + EAev'' - m\ddot{v} \\ & \quad - c_e \dot{v} + f_n^a = 0 \\ & e = -\frac{\overline{k}}{l} \int_0^l v ds + \frac{1}{2l} \int_0^l v'^2 ds \\ & v_A = 0, \\ & v_B = 0 \end{aligned} \tag{3}$$

Concerning the aerodynamic force f_n^a, we neglect the small curvature of the cable as typically done in the literature [1, 11, 24, 25]. In other words, we assume that an element of curved cable is subjected to the same aerodynamic forces which act on a long cylinder oriented as the local triad. Therefore,

$$f_z^a = \frac{1}{2} \rho U^2 b \left(\mathtt{A}_0 - \mathtt{A}_1 \left(\frac{\dot{z}}{U} \right) - \mathtt{A}_2 \left(\frac{\dot{z}}{U} \right)^2 - \mathtt{A}_3 \left(\frac{\dot{z}}{U} \right)^3 + \dots \right) \tag{4}$$

where ρ is the air density, b is a characteristic length of the cross-section, and $\mathtt{A}_i$ are aerodynamic coefficients depending on the shape of the iced cross-section, taken in average sense constant along the span. Consistently with the hypothesis of zero-static response to wind, we take $\mathtt{A}_0 = 0$.

3. The Linear Problem

In order to evaluate the critical galloping velocity U_c, the linear problem is addressed first; it reads

$$\begin{aligned} & T_0 \left(1 + \frac{\zeta}{T_0} \partial_t \right) v'' + EA\overline{k} \left(1 + \frac{\zeta}{T_0} \partial_t \right) e - m\ddot{v} \\ & \quad - \left(c_e + U_c \widehat{c}_{a1} \right) \dot{v} = 0 \\ & e + \frac{\overline{k}}{l} \int_0^l v ds = 0 \\ & v_A = 0, \\ & v_B = 0 \end{aligned} \tag{5}$$

where $\widehat{c}_{a1} := (1/2)\rho b \mathtt{A}_1$.

3.1. The Space Eigenvalue Problem. By taking into account the periodicity of motion at the bifurcation, we separate the variables, via $v(s,t) = \widehat{v}(s) \exp(i\omega_c t), e(t) = \widehat{e} \exp(i\omega_c t)$, with ω_c being the unknown frequency. A space eigenvalue problem follows:

$$\begin{aligned} & \widehat{v}'' + \frac{EA\overline{k}}{T_0} \widehat{e} + \beta^2 \widehat{v} = 0 \\ & \widehat{e} + \frac{\overline{k}}{l} \int_0^l \widehat{v} ds = 0 \\ & \widehat{v}_A = 0, \\ & \widehat{v}_B = 0 \end{aligned} \tag{6}$$

where we define the following.

$$\beta^2 := \frac{m\omega_c^2 - i\omega_c \left(c_e + U_c \widehat{c}_{a1} \right)}{T_0 \left(1 + i \left(\zeta / T_0 \right) \omega_c \right)} \tag{7}$$

This problem is formally identical to that governing the linear free oscillations of a cable [6], except for the definition of β. Therefore, $(\widehat{v}(s), \widehat{e}) = (\widehat{v}_j(s), \widehat{e}_j), j = 1, 2, \dots$, is the jth natural mode (symmetric or antisymmetric), and $\beta = \beta_j$ is the associated wave-number which solves the characteristic equation, i.e., $\sin(\beta l/2) = 0$ in the antisymmetric case, or the transcendental Irvine equation [6]

$$\tan \left(\frac{\beta l}{2} \right) = - \left(\frac{\beta l}{2} \right)^3 \frac{4}{\lambda^2} + \left(\frac{\beta l}{2} \right) \tag{8}$$

in the symmetric case, where $\lambda = \sqrt{EA(\overline{k}l)^2/T_0}$. Once β_j is known, by separating real and imaginary parts in (7), we get the two unknowns (with index denoting the jth root).

$$\begin{aligned} & U_{cj} = \frac{c_e + \zeta \beta_j^2}{\left| \widehat{c}_{a1} \right|}, \quad \widehat{c}_{a1} < 0 \\ & \omega_{cj} = \beta_j \sqrt{\frac{T_0}{m}} \end{aligned} \tag{9}$$

Since $U_c := \min_j U_{cj} = U_{c1}$, according to this model, the cable gallops in its first natural mode.

From (9) the role of the internal damping ζ clearly emerges. It splits the coalescence of infinitely many critical velocities, each associated with different natural mode, which

would manifest themselves simultaneously if the cable were non-internally damped. Such a case, however, is quite unrealistic, since it would entail the modal damping ratio decreases as $1/\omega_j$. Such a circumstance is obscured in discrete models, where different damping ratios are attributed to the natural modes on an heuristic basis, without any derivation from a model.

3.2. The Adjoint Eigenvalue Problem and the Solvability Condition. In view of a nonlinear perturbation analysis, we need the adjoint problem of (6), together with the solvability condition for the following nonhomogeneous problem:

$$\begin{aligned} &\widehat{v}'' + \frac{EA\overline{k}}{T_0}\widehat{e} + \beta^2\widehat{v} = f(s) \\ &\widehat{e} + \frac{\overline{k}}{l}\int_0^l \widehat{v}ds = \nu \\ &\widehat{v}_A = 0, \\ &\widehat{v}_B = 0 \end{aligned} \tag{10}$$

in which $f(s)$, ν are known terms. To this end, it is convenient to recast it in the integrodifferential form:

$$\begin{aligned} &\phi'' + \beta^2\phi - \frac{EA\overline{k}^2}{T_0 l}\int_0^l \phi ds = f(s) - \frac{EA\overline{k}}{T_0}\nu \\ &\phi_A = 0, \\ &\phi_B = 0 \end{aligned} \tag{11}$$

in which, for notational convenience, we define $\phi \coloneqq \widehat{v}(s)$.

The relevant Extended Green Identity then reads as follows.

$$\begin{aligned} &\int_0^l \psi\left[\phi'' + \beta^2\phi - \frac{EA\overline{k}^2}{T_0 l}\int_0^l \phi(\widetilde{s})\,d\widetilde{s}\right]ds \\ &= \int_0^l \phi\left[\psi'' - \frac{EA\overline{k}^2}{T_0 l}\int_0^l \psi(\widetilde{s})\,d\widetilde{s} + \beta^2\psi\right]ds \\ &\quad + \left[\phi'\psi + \phi\psi'\right]_0^l \end{aligned} \tag{12}$$

We conclude that problem (6) is self-adjoint, entailing $\psi \equiv \phi$. Moreover, the solvability condition reads as follows.

$$\int_0^l \phi(s)\left(f(s) - \frac{EA\overline{k}}{T_0}\nu\right)ds = 0 \tag{13}$$

4. The Nonlinear Problem

To investigate the behavior of the cable in the nonlinear field and close to the dynamic bifurcation, we carry out a nonlinear analysis. The equation governing the motion is

$$\begin{aligned} &T_0\left(1 + \frac{\zeta}{T_0}\partial_t\right)v'' + EA\overline{k}\left(1 + \frac{\zeta}{T_0}\partial_t\right)e - m\ddot{v} \\ &\quad - \left(c_e + U\widehat{c}_{a1}\right)\dot{v} + EAev'' - \widehat{c}_{a2}\dot{v}^2 - \frac{\widehat{c}_{a3}}{U}\dot{v}^3 = 0 \\ &e = -\frac{\overline{k}}{l}\int_0^l v ds + \frac{1}{2l}\int_0^1 v'^2 ds \\ &v_A = 0, \\ &v_B = 0 \end{aligned} \tag{14}$$

where $\widehat{c}_{ak} \coloneqq (1/2)\rho b\mathbb{A}_k, (k = 1, \ldots 3)$.

4.1. Multiple Scale Analysis. To solve (14), we use the asymptotic multiple scale method [12–14]. The method consists in expanding the dependent variables in formal series of a small perturbation parameter ϵ (to be reabsorbed at the end of the procedure), as well as introducing independent time scales (fast, slow, slowest,...,). Substitution of these expansions in the nonlinear equations and separation of terms of different orders lead to linear equations being solved in sequence. Accordingly, we expand the variables and the bifurcation parameter as

$$\begin{aligned} \nu &= \epsilon\nu_1 + \epsilon^2\nu_2 + \epsilon^3\nu_3 \\ e &= \epsilon e_1 + \epsilon^2 e_2 + \epsilon^3 e_3 \\ U &= U_c + \epsilon^2 U_2 \end{aligned} \tag{15}$$

with U_c being the critical velocity, which is now a known parameter. By introducing the time scales $t_0 \coloneqq t$, $t_2 \coloneqq \epsilon^2 t$ and the consequent differentiation rules

$$\begin{aligned} \partial_t &= \partial_0 + \epsilon^2\partial_2 \\ \partial_t^2 &= \partial_0^2 + 2\epsilon^2\partial_0\partial_2 \end{aligned} \tag{16}$$

where $\partial_j \coloneqq \partial/\partial t_j$, $j = 0, 2$, the perturbation equations follow after collecting the coefficients at the various orders of ϵ.

Order ϵ:

$$\begin{aligned} &T_0\left(1 + \frac{\zeta}{T_0}\partial_0\right)v_1'' + EA\overline{k}\left(1 + \frac{\zeta}{T_0}\partial_0\right)e_1 - m\partial_0^2\nu_1 \\ &\quad - \left(c_e + U_c\widehat{c}_{a1}\right)\partial_0\nu_1 = 0 \\ &e_1 + \frac{\overline{k}}{l}\int_0^l \nu_1 ds = 0 \\ &\nu_{1A} = 0, \\ &\nu_{1B} = 0 \end{aligned} \tag{17}$$

Order ϵ^2:

$$\begin{aligned} &T_0\left(1 + \frac{\zeta}{T_0}\partial_0\right)v_2'' + EA\overline{k}\left(1 + \frac{\zeta}{T_0}\partial_0\right)e_2 - m\partial_0^2\nu_2 \\ &\quad - \left(c_e + U_c\widehat{c}_{a1}\right)\partial_0\nu_2 = \widehat{c}_{a2}\left(\partial_0\nu_1\right)^2 - EAv_1''e_1 \\ &e_2 + \frac{\overline{k}}{l}\int_0^l \nu_2 ds = \frac{1}{2l}\int_0^l v_1'^2 ds \\ &\nu_{2A} = 0, \\ &\nu_{2B} = 0 \end{aligned} \tag{18}$$

Order ϵ^3:

$$T_0\left(1+\frac{\zeta}{T_0}\partial_0\right)v_3''+EA\overline{k}\left(1+\frac{\zeta}{T_0}\partial_0\right)e_3-m\partial_0^2v_3 - \left(c_e+U_c\widehat{c}_{a1}\right)\partial_0v_3=2m\partial_0\partial_2v_1-\zeta\partial_2v_1'' - \zeta\frac{EA}{T_0}\overline{k}\partial_2e_1+\left(c_e+U_c\widehat{c}_{a1}\right)\partial_2v_1+U_2\widehat{c}_{a1}\partial_0v_1 + 2\widehat{c}_{a2}\left(\partial_0v_1\right)\left(\partial_0v_2\right)+\frac{\widehat{c}_{a3}}{U_c}\left(\partial_0v_1\right)^3 - EA\left(v_2''e_1+v_1''e_2\right) \tag{19a}$$

$$e_3+\frac{\overline{k}}{l}\int_0^l v_3ds=\frac{1}{l}\int_0^l v_1'v_2'ds \tag{19b}$$

$$v_{3A}=0, \tag{19c}$$

$$v_{3B}=0 \tag{19d}$$

By excluding internal resonances among the natural modes, the (monomodal) solution to the order ϵ reads

$$\begin{pmatrix}v_1\\e_1\end{pmatrix}=A\left(t_2\right)\begin{pmatrix}\widehat{v}_c\left(s\right)\\\widehat{e}_c\end{pmatrix}e^{i\omega_ct_0}+c.c. \tag{20}$$

where $A(t_2)$ is a complex modulating function, $(\widehat{v}_c(s),\widehat{e}_c)$ is the real critical (first in-plane natural) mode of the cable, ω_c is the associated frequency, and c.c. stands for complex conjugate.

By solving in sequence (18) and (19) and enforcing to this latter the solvability condition, the following ordinary differential equation for the amplitude is found (see the appendix for details):

$$\dot{A}=-U_2c_1A+\left(c_{3R}+ic_{3I}\right)A^2\overline{A} \tag{21}$$

which is the well-known normal form for Hopf bifurcation [26]. By letting $A(t)=(1/2)a(t)e^{i\varphi(t)}$, followed by the separation of real and imaginary parts and some algebraic manipulation, the real form of the bifurcation equation is derived.

$$\dot{a}=-U_2c_1a+\frac{c_{3R}}{4}a^3 \tag{22a}$$

$$a\dot{\varphi}=\frac{c_{3I}}{4}a^3 \tag{22b}$$

The equilibrium solutions of (22a) are $a_0=0$ (trivial motion) and $a_{1,2}=\pm2\sqrt{c_1/c_{3R}}$ (limit-cycle amplitude). An eigenvalue analysis of the same equation states that a_0 is stable for $U_2<0$ and unstable for $U_2>0$, whereas the bifurcated branches $a_{1,2}$, emanating from $U_2=0$, are stable for $U_2>0$ (i.e., the Hopf bifurcation is supercritical).

In terms of the physical variables, the motion of the cable on the limit-cycle is

$$v\left(s,t\right)=a\left(t\right)\widehat{v}_c\left(s\right)\cos\left(\omega_ct+\varphi\left(t\right)\right)+\frac{1}{2}a\left(t\right)^2 \cdot\left[\chi_{20}\left(s\right)+\chi_{22R}\left(s\right)\cos\left(2\left(\omega_ct+\varphi\left(t\right)\right)\right) -\chi_{22I}\left(s\right)\sin\left(2\left(\omega_ct+\varphi\left(t\right)\right)\right)\right] \tag{23a}$$

$$e\left(t\right)=a\left(t\right)\widehat{e}_c\cos\left(\omega_ct+\varphi\left(t\right)\right)+\frac{1}{2}a\left(t\right)^2\left[\eta_{20} +\eta_{22R}\cos\left(2\left(\omega_ct+\varphi\left(t\right)\right)\right) -\eta_{22I}\sin\left(2\left(\omega_ct+\varphi\left(t\right)\right)\right)\right] \tag{23b}$$

where quantities are defined in the appendix. The $\chi's$ functions account for the pattern modification and reveal the complex nature of the nonlinear normal mode, i.e., the deflected shape of the cable changes during a period.

5. Finite-Dimensional Models

In view of numerical applications and comparisons of results, two finite-dimensional models for galloping analysis are obtained via (i) the finite difference method and (ii) the Galerkin method.

5.1. Finite Difference Method. The space interval $[0,l]$ is divided into $N_s>2$ equispaced subintervals of amplitude $\Delta=l/N_s$. The following notation is adopted:

$$\begin{aligned}&s_j:=j\Delta,\quad j=0,1,\ldots,N_s,\\&v_j:=v\left(s_j,t\right),\quad j=0,1,\ldots,N_s,\\&v_j':=v'\left(s_j,t\right),\quad j=0,1,\ldots,N_s.\end{aligned} \tag{24}$$

By computing the integral via the trapezoidal rule and the space derivatives via the central finite differences, the equations in (14) become

$$\begin{aligned}&m\ddot{v}_j+\left(c_e+U\widehat{c}_{a1}\right)\dot{v}_j-\zeta\frac{\dot{v}_{j+1}-2\dot{v}_j+\dot{v}_{j-1}}{\Delta^2}+\widehat{c}_{a2}\dot{v}_j^2 +\frac{\widehat{c}_{a3}}{U}\dot{v}_j^3\\&=\left(T_0+EAe\right)\frac{v_{j+1}-2v_j+v_{j-1}}{\Delta^2} +EA\overline{k}\left(e+\frac{\zeta}{T_0}\dot{e}\right),\quad j=1,\ldots,N_s-1,\end{aligned} \tag{25}$$

in which

$$\begin{aligned}e&=-\frac{\Delta\overline{k}}{l}\sum_{k=1}^{N_s-1}v_k+\frac{1}{4l\Delta}\left[v_1^2+v_{N_s-1}^2 +\frac{1}{2}\sum_{k=1}^{N_s-1}\left(v_{k+1}-v_{k-1}\right)^2\right],\\\dot{e}&=-\frac{\Delta\overline{k}}{l}\sum_{k=1}^{N_s-1}\dot{v}_k+\frac{1}{2l\Delta}\left\{v_1\dot{v}_1+v_{N_s-1}\dot{v}_{N_s-1} +\frac{1}{2}\sum_{k=1}^{N_s-1}\left[\left(v_{k+1}-v_{k-1}\right)\left(\dot{v}_{k+1}-\dot{v}_{k-1}\right)\right]\right\},\\v_0&=v_{N_s}=0.\end{aligned} \tag{26}$$

Here, in computing e (and $\dot{e}$) the space derivatives of the displacement at $s=0,l$ were evaluated as

$$\begin{aligned}v_0'&=\frac{v_1}{\Delta},\\v_{N_s}'&=-\frac{v_{N_s-1}}{\Delta},\end{aligned} \tag{27}$$

via forward and backward finite differences, respectively, by taking into account $v_0 = v_{N_s} = 0$.

Equations (25) are a set of $N_s - 1$ ordinary differential equations for the unknown nodal displacements $v_j(t)$, $j = 1, \ldots, N_s - 1$.

5.2. Galerkin Method. The transverse displacement is assumed as the truncated series:

$$v(s,t) = \sum_{j=1}^{N_e} \phi_j(s)\, q_j(t), \tag{28}$$

where q_j are generalized coordinates and

$$\phi_j(s) = \sqrt{\frac{2}{ml}} \sin\left(\frac{j\pi}{l} s\right) \tag{29}$$

are trial functions satisfying

$$\begin{aligned} \int_0^l \phi_i \phi_j ds &= \frac{1}{m}\delta_{ij}, \\ \int_0^l \phi_i' \phi_j' ds &= \frac{1}{m}\left(\frac{j\pi}{l}\right)^2 \delta_{ij}, \end{aligned} \tag{30}$$

in which δ_{ij} is the Kronecker symbol.

By substituting the expansion (28) in the governing equation (14), weighting the residual of the partial differential equation via the same trial functions ϕ_i, and using the orthonormalization properties (30), the following equations are obtained:

$$\begin{aligned} &\ddot{q}_i + \frac{1}{m}\left[\zeta\left(\frac{i\pi}{l}\right)^2 + c_e + U\hat{c}_{a1}\right]\dot{q}_i \\ &\quad + \frac{T_0 + EAe}{m}\left(\frac{i\pi}{l}\right)^2 q_i \\ &\quad - \left(\frac{1 + (-1)^{i+1}}{i}\right)\frac{l}{\pi}\sqrt{\frac{2}{ml}}EA\bar{k}\left(e + \frac{\zeta}{T_0}\dot{e}\right) \\ &\quad + \hat{c}_{a2}\sum_{j=1}^{N_e}\sum_{h=1}^{N_e}\left(\Gamma_{ijh}\dot{q}_j\dot{q}_h\right) \\ &\quad + \frac{\hat{c}_{a3}}{U}\sum_{j=1}^{N_e}\sum_{h=1}^{N_e}\sum_{k=1}^{N_e}\left(\Gamma_{ijhk}\dot{q}_j\dot{q}_h\dot{q}_k\right) = 0, \\ &\qquad\qquad\qquad\qquad\qquad\qquad i = 1, \ldots, N_e, \end{aligned} \tag{31}$$

where

$$\begin{aligned} e &= -\frac{\bar{k}}{\pi}\sqrt{\frac{2}{ml}}\sum_{h=1}^{N_e}\left(\frac{1 + (-1)^{h+1}}{h} q_h\right) + \frac{\pi^2}{2ml^3}\sum_{h=1}^{N_e}\left(h^2 q_h^2\right), \\ \dot{e} &= -\frac{\bar{k}}{\pi}\sqrt{\frac{2}{ml}}\sum_{h=1}^{N_e}\left(\frac{1 + (-1)^{h+1}}{h} \dot{q}_h\right) + \frac{\pi^2}{ml^3}\sum_{h=1}^{N_e}\left(h^2 q_h \dot{q}_h\right), \end{aligned}$$

$$\Gamma_{ijh} \coloneqq \begin{cases} 0 & \begin{array}{l} i = j + h, \\ \text{or } j = i + h, \\ \text{or } h = i + j \end{array} \\ \dfrac{4}{\pi}\sqrt{\dfrac{2}{m^3 l}}\dfrac{\left[(-1)^{i+j+h} - 1\right] ijh}{(i + j + h)(i - j + h)(i + j - h)(i - j - h)} & \text{otherwise} \end{cases} \tag{32}$$

$$\Gamma_{ijhk} \coloneqq \begin{cases} \dfrac{3}{2m^2 l} & i = j = h = k \\ -\dfrac{1}{2m^2 l} & \begin{array}{l} i = j + h + k, \text{ or } j = i + h + k, \\ \text{or } h = i + j + k, \text{ or } k = i + j + h \end{array} \\ \dfrac{1}{2m^2 l} & \begin{array}{l} i + j = h + k,\ j \neq h,\ j \neq k \\ \text{or } i + h = j + k,\ h \neq j,\ h \neq k \\ \text{or } j + h = i + k,\ h \neq i,\ h \neq k \end{array} \\ \dfrac{1}{m^2 l} & i = j, h = k, \text{ or } i = h, j = k, \text{ or } i = k, j = h \\ 0 & \text{otherwise.} \end{cases}$$

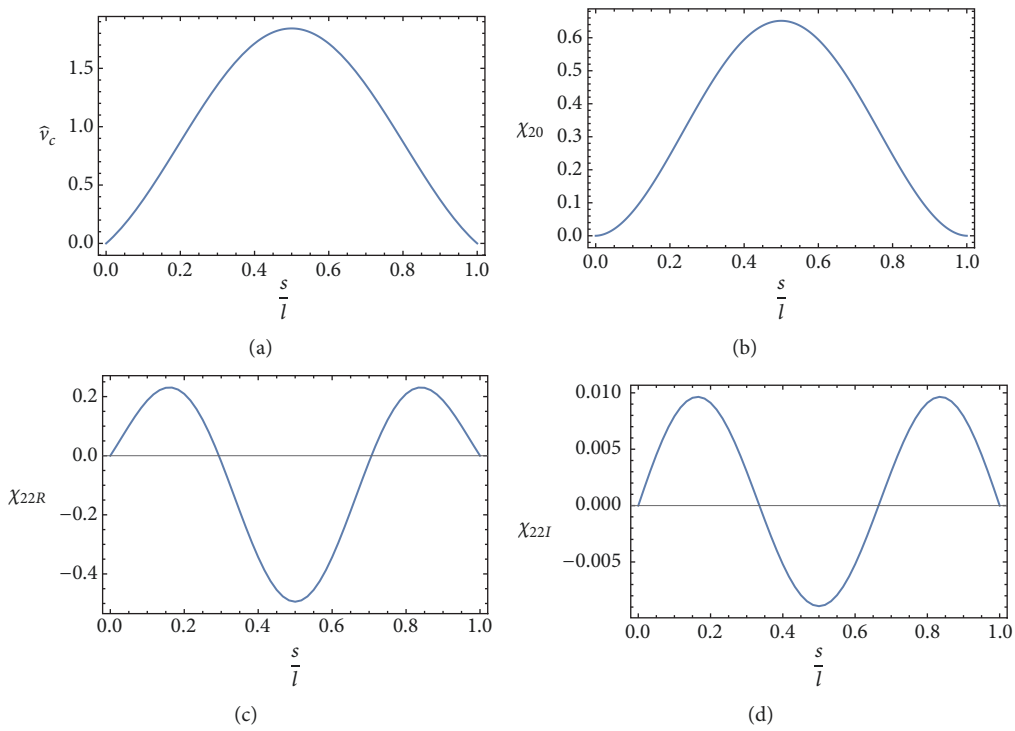

FIGURE 2: Case-study 1: symmetric mode and second order corrections.

Equations (31) are a set of N_e ordinary differential equations for the generalized coordinates $q_j(t)$, $j = 1, \ldots, N_e$.

6. Numerical Results

A cable of the following geometrical and mechanical characteristic is considered: $m = 1.80$ kg/m, $l = 267$ m, $EA = 2.97 \times 10^7$ N. The internal damping coefficient is $c_e = 0.022$ kg/(ms) and the external one is $\zeta = 48.939$ kgm/s.

The aerodynamic parameters are taken from [24, 25], where an U-shaped conductor is considered, with its maximum ice eccentricity aligned to the mean wind velocity. The drag and lift coefficients are

$$c_d(\gamma) = 1.08334 + 0.735935\gamma^2$$
$$c_l(\gamma) = -1.5979\gamma + 4.77362\gamma^3 \tag{33}$$

with γ being the angle of attack (evaluated in the cross-section plane and formed between the unit vector $\mathbf{a}_b$ and wind axis $\mathbf{a}_z$) and assumed valid in the range $-0.6 < \gamma < 0.6$ rad. Furthermore, the air mass per unit volume is $\rho = 1.25$ kg/m^3 and the cable mean diameter is $b = 0.0281$ m.

Two case-studies are considered, differing from each other in the sag $d \simeq mgl^2/8T_0$: (1) the cable is below the first cross-over condition ($d = 5$ m, and consequently $\lambda = 4.602 < 2\pi$); (2) the cable is above the first cross-over condition ($d = 7.0$ m, and consequently $\lambda = 7.624 > 2\pi$).

In case-study (1), the first linear mode is symmetric (Figure 2(a)), the dynamic unitary extension is $\widehat{e}_c = -5.901 \times 10^{-4}$, and the critical conditions, as obtained from (9), are $\omega_c = 2.547$ rad/s and $U_c = 4.465$ m/s. The second order corrections to the modal shape $\chi_{20}(s)$, $\chi_{22R}(s)$, and $\chi_{22I}(s)$ are shown in Figures 2(b)–2(d) and the corrections to the dynamic unitary extension are $\eta_{20} = -7.939 \times 10^{-5}$, $\eta_{22R} = 1.314 \times 10^{-4}$, and $\eta_{22I} = 1.255 \times 10^{-6}$.

The obtained bifurcation diagram is shown in Figure 3(a), where the classical supercritical Hopf bifurcation behavior is evident, whereas the space and time postcritical evolution of the cable is shown in Figure 3(b), as obtained from (23a), for $U_2/U_c = 0.11$.

A comparison of the time evolution of the cable for the same postcritical condition $U_2/U_c = 0.11$ is shown in Figure 4, where the displacements at half-span and quarter-span, as obtained from MSM (green line), Galerkin method with $N_e = 20$ (blue line), and finite difference method with $N_s = 100$ (orange line), are in good agreement, highlighting the reliability of the asymptotic procedure. The phase plots, shown in Figure 5 for half-span and quarter-span, exhibit feeble modification of the elliptical form and highlight the slight modification of the oscillation shape during a period, due to the nonlinear contributions.

In case (2), the first linear mode is antisymmetric (Figure 6(a)), the dynamic unitary extension is $\widehat{e}_c = 0$, and the critical conditions, as obtained from (9), are $\omega_c = 2.630$ rad/s and $U_c = 5.454$ m/s. The second order corrections to the modal shape $\chi_{20}(s)$, $\chi_{22R}(s)$, and $\chi_{22I}(s)$ are shown in Figures 6(b)–6(d) and the dynamic unitary extension is corrected by $\eta_{20} = 2.369 \times 10^{-5}$, $\eta_{22R} = 2.191 \times 10^{-4}$, and $\eta_{22I} = 1.643 \times 10^{-6}$.

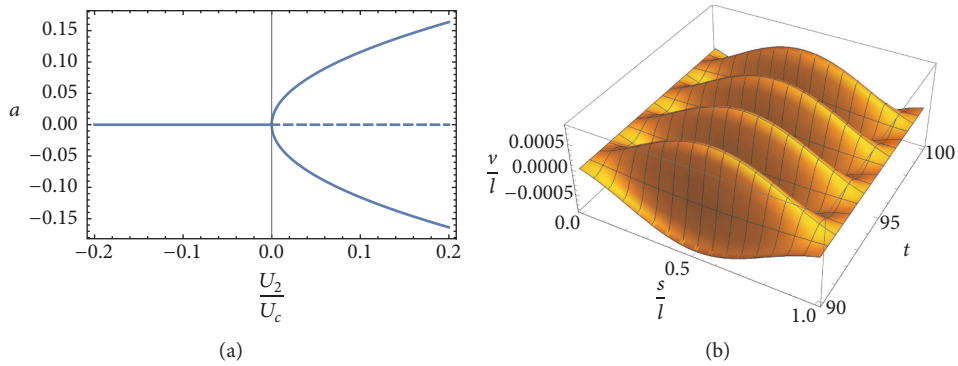

(a) (b)

Figure 3: Case-study 1: (a) bifurcation diagram (solid line: stable; dashed line: unstable); (b) reconstituted displacement $v(s,t)$ of the cable for $U_2/U_c = 0.11$.

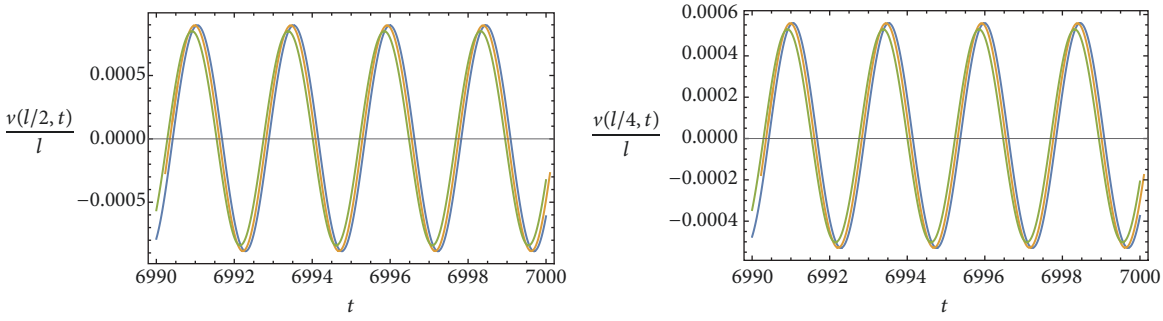

(a) (b)

Figure 4: Case-study 1: reconstituted time evolution of the displacement $v(s,t)$ for $U_2/U_c = 0.11$ at (a) half-span and (b) quarter-span (green line: multiple scale method; blue line: Galerkin method; orange line: finite difference method).

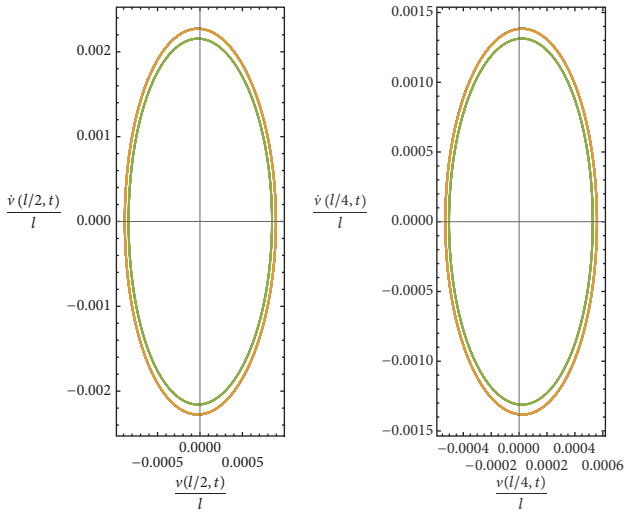

(a) (b)

Figure 5: Case-study 1: reconstituted phase plot $(v, \dot{v})$ for $U_2/U_c = 0.11$ at (a) half-span and (b) quarter-span (green line: multiple scale method; blue line: Galerkin method; orange line: finite difference method).

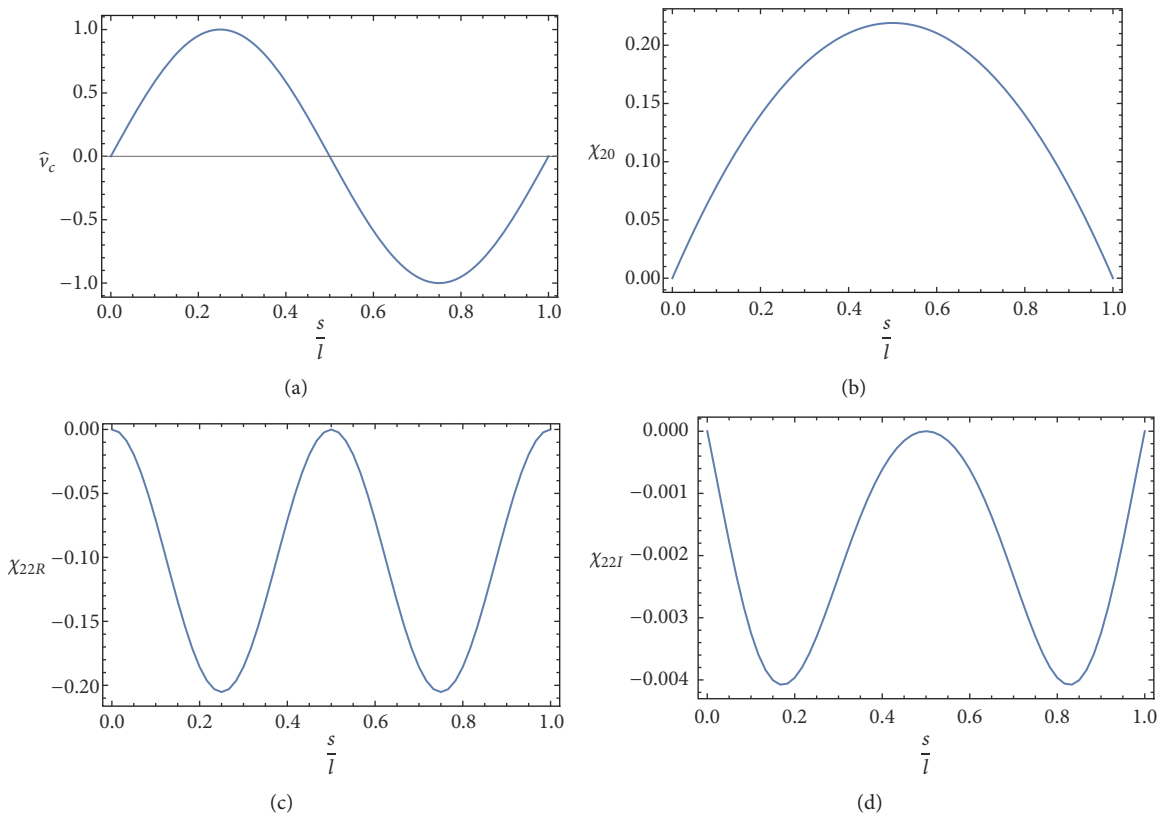

FIGURE 6: Case-study 2: antisymmetric mode and second order corrections.

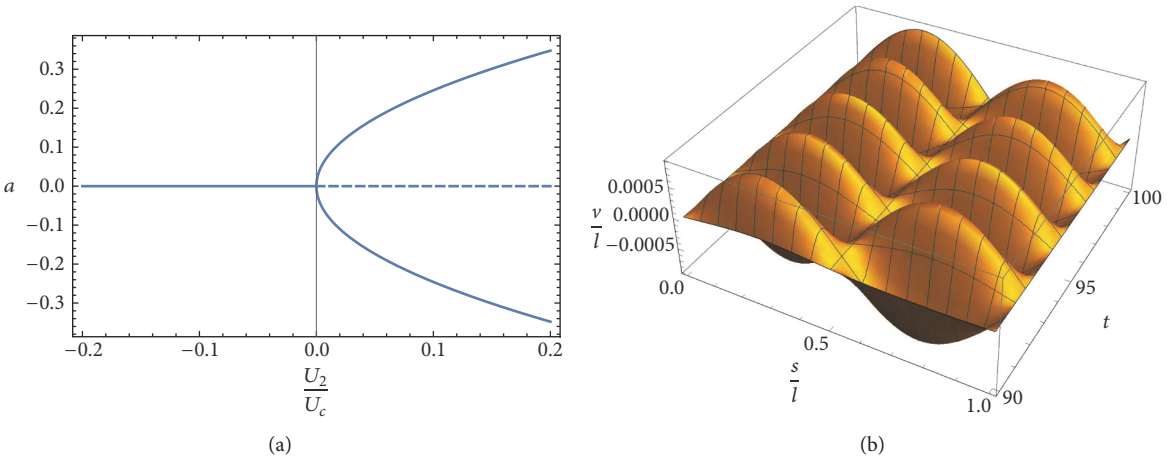

FIGURE 7: Case-study 2: (a) bifurcation diagram (solid line: stable; dashed line: unstable); (b) reconstituted displacement $v(s,t)$ of the cable for $U_2/U_c = 0.09$.

The obtained bifurcation diagram is shown in Figure 7(a), where still the classical Hopf bifurcation behavior is obtained, whereas the space and time postcritical evolution of the cable is shown in Figure 7(b), as obtained from (23a), for $U_2/U_c = 0.09$.

The comparison of the time evolution of the cable for $U_2/U_c = 0.09$ is shown in Figure 8, where the displacements at half-span and quarter-span, as obtained from MSM (green line), Galerkin method with $N_e = 20$ (blue line), and finite difference method with $N_s = 100$ (orange line), are in good agreement, highlighting the reliability of the asymptotic procedure. Moreover, in Figure 8(a) the prevalent contribution of the static drift due to the quadratic nonlinearities is evident. The phase plot at the quarter-span, shown in Figure 9, highlights the slight modification of the oscillation pattern during a period, due to the nonlinear contributions.

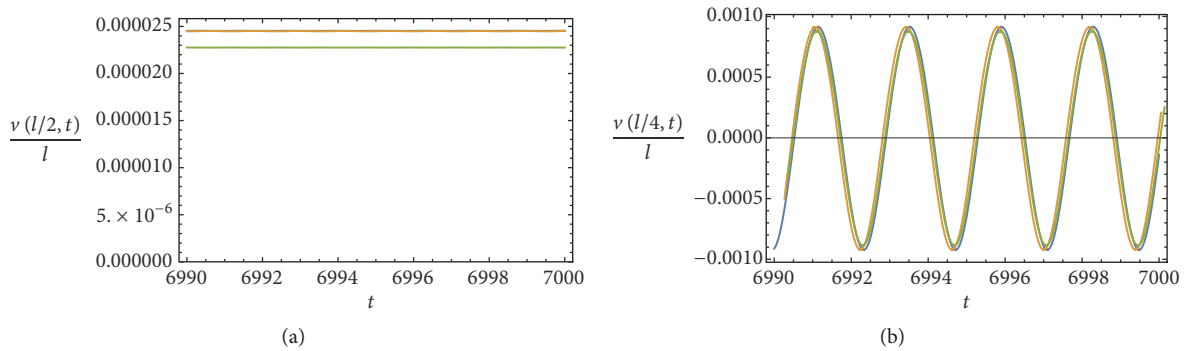

FIGURE 8: Case-study 2: reconstituted time evolution of the displacement $v(s,t)$ for $U_2/U_c = 0.09$ at (a) half-span and (b) quarter-span (green line: multiple scale method; blue line: Galerkin method; orange line: finite difference method).

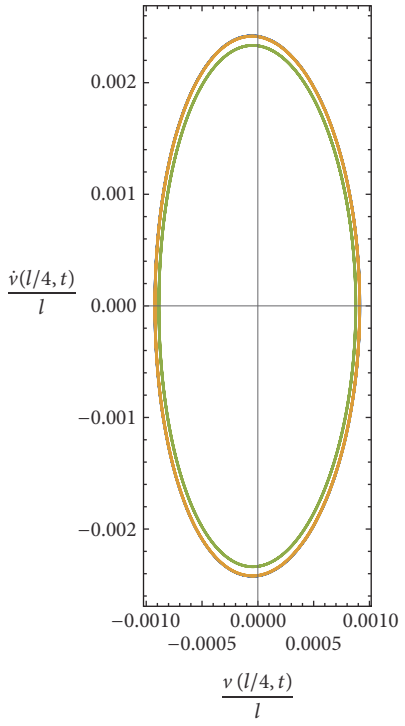

FIGURE 9: Case-study 2: reconstituted phase plot $(v, \dot{v})$ for $U_2/U_c = 0.09$ at quarter-span (green line: multiple scale method; blue line: Galerkin method; orange line: finite difference method).

7. Conclusions

Monomodal galloping of horizontal cables is addressed in the paper in a direct approach to a continuum model of flexible cable. Besides the classical external damping, an internal damping contribution is considered in the spirit of the Rayleigh model. In particular, it is related to the viscoelastic behavior of the material and is taken as proportional to the stiffness operator. Its contribution to the critical conditions of galloping is analyzed, as it turns out that it splits the critical wind velocities associated with each mode. Moreover, the postcritical behavior is addressed through the nonlinear problem, evaluating the shape modifications of the critical mode and the amplitude of the limit-cycle; this is carried out directly applying a perturbation method to the partial differential equations of motion. Numerical results are shown with regard to two case-studies, far from the cross-over point, where the critical mode is of symmetric or antisymmetric form, respectively. They are in good agreement with outcomes of relevant finite-dimensional models obtained via the application of the finite difference method or the Galerkin method. The effect of the internal damping term turns out to be essential in the evaluation of the critical velocity, and it participates in the definition of the shape modification.

Appendix

Details on Perturbation Analysis

With the generating solution (20), the ϵ^2-order perturbation equation (18) admits the solution

$$\begin{aligned} v_2 &= A^2 \chi_{22}(s) \exp\left(2i\omega_c t_0\right) + A\overline{A}\chi_{20}(s) + \text{c.c.} \\ e_2 &= A^2 \eta_{22} \exp\left(2i\omega_c t_0\right) + A\overline{A}\eta_{20} + \text{c.c.} \end{aligned} \tag{A.1}$$

where the (complex) function $\chi_{22}(s)$ and constant η_{22} solve the following boundary value problem:

$$\begin{aligned} & T_0\left(1 + 2i\omega_c \frac{\zeta}{T_0}\right)\chi_{22}'' + EA\overline{k}\left(1 + 2i\omega_c \frac{\zeta}{T_0}\right)\eta_{22} \\ & \quad + \left(4m\omega_c^2 - 2i\omega_c c_e - 2i\omega_c U_c \widehat{c}_{a1}\right)\chi_{22} = -\omega_c^2 \widehat{c}_{a2}\widehat{v}_c^2 \\ & \quad - EA\widehat{v}_c''\widehat{e}_c \\ & \eta_{22} + \frac{\overline{k}}{l}\int_0^l \chi_{22} ds = \frac{1}{2l}\int_0^l \widehat{v}_c'^2 ds \\ & \chi_{22A} = 0, \\ & \chi_{22B} = 0 \end{aligned} \tag{A.2}$$

and the (real) function $\chi_{20}(s)$ and constant η_{20} solve the following one.

$$\begin{aligned} T_0\chi_{20}'' + EA\overline{k}\eta_{20} &= -EA\widehat{v}_c''\widehat{e}_c + \omega_c^2\widehat{c}_{a2}\widehat{v}_c^2 \\ \eta_{20} + \frac{\overline{k}}{l}\int_0^l \chi_{20}ds &= \frac{1}{2l}\int_0^l \widehat{v}_c'^2 ds \\ \chi_{20A} &= 0, \\ \chi_{20B} &= 0 \end{aligned} \tag{A.3}$$

By going ahead to the ϵ^3-order equation (19), the solvability condition (13) must be enforced. To this end, we substitute the integral expression for e_3 (19b) into the field equation (19a) and formulate this latter into the integrodifferential form (11):

$$\begin{aligned} &T_0\left(1+\frac{\zeta}{T_0}\partial_0\right)v_3'' - \frac{EA\overline{k}^2}{l}\left(1+\frac{\zeta}{T_0}\partial_0\right)\int_0^l v_3 ds \\ &\quad - m\partial_0^2 v_3 - \left(c_e + U_c\widehat{c}_{a1}\right)\partial_0 v_3 \\ &= \left(q(s,t_2) - EA\overline{k}\left(1+i\omega_c\frac{\zeta}{T_0}\right)\nu(t_2)\right)e^{i\omega_c t_0} \\ &\quad + \text{NRT} + \text{c.c.} \end{aligned} \tag{A.4}$$

where NRT stands for nonresonant terms and

$$\begin{aligned} q(s,t_2) \coloneqq\ & i\widehat{c}_{a1}U_2\omega_c A\widehat{v}_c + \frac{3i\widehat{c}_{a3}}{U_c}\omega_c^3 A^2\overline{A}\widehat{v}_c^3 \\ &+ 4\widehat{c}_{a2}\omega_c^2 A^2\overline{A}\widehat{v}_c\chi_{22} - \frac{EA\widehat{e}_c\overline{k}\zeta}{T_0}A' \\ &+ \left(c_e + \widehat{c}_{a1}U_c + 2im\omega_c\right)A'\widehat{v}_c - \zeta A'\widehat{v}_c'' \\ &- EA\left(2\eta_{20} + \eta_{22}\right)A^2\overline{A}\widehat{v}_c'' \\ &- EA\widehat{e}_c A^2\overline{A}\left(2\chi_{20}'' + \chi_{22}''\right) \\ \nu(t_2) \coloneqq\ & \frac{A^2\overline{A}}{l}\int_0^l \widehat{v}_c'\left(2\chi_{20}' + \chi_{22}'\right)ds. \end{aligned} \tag{A.5}$$

Solvability then requires that the known term of this latter is orthogonal to $\widehat{v}_c(s)$, i.e.,

$$\begin{aligned} &\int_0^l \widehat{v}_c(s)\, q(s,t_2)\, ds \\ &\quad - EA\overline{k}\left(1+i\omega_c\frac{\zeta}{T_0}\right)\nu(t_2)\int_0^l \widehat{v}_c(s)\, ds = 0. \end{aligned} \tag{A.6}$$

This latter, after backward resorting to the true time, supplies the bifurcation equation (21). In it, the following positions hold:

$$\begin{aligned} c_1 &= \frac{\widehat{c}_{a1}}{2m}, \\ c_{3R} &= -\frac{1}{2m\omega_c\int_0^l \widehat{v}_c^2 ds}\left[\frac{3\widehat{c}_{a3}\omega_c^3}{U_c}\int_0^l \widehat{v}_c^4 ds\right. \\ &\quad + 4\widehat{c}_{a2}\omega_c^2\int_0^l \widehat{v}_c^2\chi_{22I}ds - \frac{EA\overline{k}}{l}\int_0^l \widehat{v}_c ds \\ &\quad \cdot\left(\frac{\zeta\omega_c}{T_0}\int_0^l \widehat{v}_c'\left(2\chi_{20}' + \chi_{22R}'\right)ds + \int_0^l \widehat{v}_c'\chi_{22I}'ds\right) \\ &\quad \left. - EA\eta_{22I}\int_0^l \widehat{v}_c\widehat{v}_c''ds - EA\widehat{e}_c\int_0^l \widehat{v}_c\chi_{22I}''ds\right] \\ c_{3I} &= \frac{1}{2m\omega_c\int_0^l \widehat{v}_c^2 ds}\left[4\widehat{c}_{a2}\omega_c^2\int_0^l \widehat{v}_c^2\chi_{22R}ds - \frac{EA\overline{k}}{l}\right. \\ &\quad \cdot\int_0^l \widehat{v}_c ds \\ &\quad \cdot\left(\frac{\zeta\omega_c}{T_0}\int_0^l \widehat{v}_c'\chi_{22I}'ds - \int_0^l \widehat{v}_c'\left(\chi_{22R}' + 2\chi_{20}'\right)ds\right) \\ &\quad - EA\left(\eta_{22R} + 2\eta_{20}\right)\int_0^l \widehat{v}_c\widehat{v}_c''ds \\ &\quad \left. - EA\widehat{e}_c\int_0^l \widehat{v}_c\left(\chi_{22R}'' + 2\chi_{20}''\right)ds\right] \end{aligned} \tag{A.7}$$

and $\chi_{22}(s) = \chi_{22R}(s) + i\chi_{22I}(s), \eta_{22} = \eta_{22R} + i\eta_{22I}$.

Data Availability

The data used to support the findings of this study are available from the corresponding author upon request.

Conflicts of Interest

The authors declare that they have no conflicts of interest.

References

[1] J. P. Den Hartog, *Mechanical Vibrations*, Dover Publications, 1985.

[2] A. Luongo and G. Piccardo, "Linear instability mechanisms for coupled translational galloping," *Journal of Sound and Vibration*, vol. 288, no. 4-5, pp. 1027–1047, 2005.

[3] C. L. Lee and N. C. Perkins, "Nonlinear oscillations of suspended cables containing a two-to-one internal resonance," *Nonlinear Dynamics*, vol. 3, no. 6, pp. 465–490, 1992.

[4] A. Luongo and D. Zulli, "Dynamic instability of inclined cables under combined wind flow and support motion," *Nonlinear Dynamics*, vol. 67, no. 1, pp. 71–87, 2012.

[5] A. Luongo and G. Piccardo, "A continuous approach to the aeroelastic stability of suspended cables in 1:2 internal resonance," *Journal of Vibration and Control*, vol. 14, no. 1-2, pp. 135–157, 2008.

[6] H. M. Irvine, *Cable Structures*, MiT Press, Cambridge, UK, 1981.

[7] G. Rega, "Nonlinear vibrations of suspended cables—part I: modeling and analysis," *Applied Mechanics Reviews*, vol. 57, no. 1-6, pp. 443–478, 2004.

[8] G. Rega, "Nonlinear vibrations of suspended cables—part II: deterministic phenomena," *Applied Mechanics Reviews*, vol. 57, no. 6, pp. 479–514, 2004.

[9] A. Luongo and D. Zulli, "Parametric, external and self-excitation of a tower under turbulent wind flow," *Journal of Sound and Vibration*, vol. 330, no. 13, pp. 3057–3069, 2011.

[10] D. Zulli and A. Luongo, "Bifurcation and stability of a two-tower system under wind-induced parametric, external and self-excitation," *Journal of Sound and Vibration*, vol. 331, no. 2, pp. 365–383, 2012.

[11] F. Foti and L. Martinelli, "A unified analytical model for the self-damping of stranded cables under aeolian vibrations," *Journal of Wind Engineering & Industrial Aerodynamics*, vol. 176, pp. 225–238, 2017.

[12] A. H. Nayfeh, *Introduction to Perturbation Techniques*, John Wiley & Sons, New York, NY, USA, 2001.

[13] A. H. Nayfeh, *Perturbation Methods*, John Wiley & Sons, New York, NY, USA, 2000.

[14] A. H. Nayfeh and D. T. Mook, *Nonlinear Oscillations*, John Wiley & Sons, New York, NY, USA, 2008.

[15] A. Luongo and D. Zulli, "Statics of shallow inclined elastic cables under general vertical loads: A perturbation approach," *Mathematics*, vol. 6, no. 2, pp. 63–72, 2018.

[16] A. Luongo and D. Zulli, "Static Perturbation Analysis of Inclined Shallow Elastic Cables under general 3D-loads," *Curved and Layered Structures*, vol. 5, pp. 250–259, 2018.

[17] H. M. Irvine and T. K. Caughey, "The Linear Theory of Free Vibrations of a Suspended Cable," *Proceedings of the Royal Society A Mathematical, Physical and Engineering Sciences*, vol. 341, no. 1626, pp. 299–315, 1974.

[18] P. Hagedorn and B. Schäfer, "On non-linear free vibrations of an elastic cable," *International Journal of Non-Linear Mechanics*, vol. 15, no. 4-5, pp. 333–340, 1980.

[19] N. C. Perkins, "Modal interactions in the non-linear response of elastic cables under parametric/external excitation," *International Journal of Non-Linear Mechanics*, vol. 27, no. 2, pp. 233–250, 1992.

[20] V. V. Bolotin, *Nonconservative Problems of The Theory of Elastic Stability*, Macmillan, 1963.

[21] O. N. Kirillov and A. P. Seyranian, "The effect of small internal and external damping on the stability of distributed non-conservative systems," *Journal of Applied Mathematics and Mechanics*, vol. 69, no. 4, pp. 529–552, 2005.

[22] M. Tommasini, O. N. Kirillov, D. Misseroni, and D. Bigoni, "The destabilizing effect of external damping: Singular flutter boundary for the Pflüger column with vanishing external dissipation," *Journal of the Mechanics and Physics of Solids*, vol. 91, pp. 204–215, 2016.

[23] R. W. Clough and J. Penzien, *Dynamics of Structures*, Comput. Struct., Inc, Berkeley, calif, USA, 3rd edition, 2003.

[24] P. Yu, M. Desai, A. H. Shah, and N. Popplewell, "Three-degree-of-freedom model for galloping. Part I: formulation," *Journal of Engineering Mechanics*, vol. 119, no. 12, pp. 2404–2425, 1993.

[25] P. Yu, Y. M. Desai, N. Popplewell, and A. H. Shah, "Three-degree-of-freedom model for galloping. Part II: Solutions," *Journal of Engineering Mechanics*, vol. 119, no. 12, pp. 2426–2448, 1993.

[26] J. Guckenheimer and P. Holmes, *Nonlinear Oscillations, Dynamical Systems, and Bifurcation of Vector Fields*, Springer, New York, NY, USA, 1983.